SF 298 MASTER COPY KEEP THIS COPY FOR REPRODUCTION PURPOSES

REPORT DOCUMENTATION PAGE

Form Approved
OMB NO. 0704-0188

1. AGENCY USE ONLY (Leave blank)	2. REPORT DATE	3. REPORT TYPE AND DATES COVERED
	June 9, 1997	Final Report 9/91 - 9/94

4. TITLE AND SUBTITLE

Nanocomposites Synthesized by High Pressure Injection of Porous Dielectrics as Optical Materials

5. FUNDING NUMBERS

29671-MS-H

and/or DAAL03-91-G-0340

DAAL03-91-G-0340

6. AUTHOR(S)

Tito E. Huber

7. PERFORMING ORGANIZATION NAMES(S) AND ADDRESS(ES)

Howard University
2400 Sixth Street, N.W.
O.O. Box 1071, Washington, DC 20059

8. PERFORMING ORGANIZATION REPORT NUMBER

9. SPONSORING / MONITORING AGENCY NAME(S) AND ADDRESS(ES)

U.S. Army Research Office
P.O. Box 12211
Research Triangle Park, NC 27709-2211

10. SPONSORING / MONITORING AGENCY REPORT NUMBER

ARO 29671.7-MS-H

11. SUPPLEMENTARY NOTES

The views, opinions and/or findings contained in this report are those of the author(s) and should not be construed as an official Department of the Army position, policy or decision, unless so designated by other documentation.

12a. DISTRIBUTION / AVAILABILITY STATEMENT

Approved for public release: distribution unlimited.

12 b. DISTRIBUTION CODE

13. ABSTRACT (Maximum 200 words)

This research focuses on dense conductor-dielectric nanocomposites, i.e., composites in which the conducting phase occupies a volume fraction of several tens percent. Many applications, especially those involving electrical transport, call for a high concentration of the active conducting phase. We have developed a high pressure-high temperature injection technique for the synthesis of composites using nanochannel dielectrics as templates. Using this technique, we have prepared and characterized two distinct type of composites: nanocrystalline networks and nanowire arrays. We have performed structural, optical and transport measurements which highlight the role of the microstructure on the electronic properties of the composites. The nanowire composites have been used as prototype materials for the development of a scanning electric force microscope by a company specializing in scanning force microscopes. They can also be utilized as building blocks for high density multifeedthroughs and photosensing arrays; three patents have been filed for these applications.

14. SUBJECT TERMS

composites, nanowires, electric force microscope

15. NUMBER IF PAGES 20

16. PRICE CODE

17. SECURITY CLASSIFICATION OF REPORT	18. SECURITY CLASSIFICATION OF THIS PAGE	19. SECURITY CLASSIFICATION OF ABSTRACT	20. LIMITATION OF ABSTRACT
UNCLASSIFIED	UNCLASSIFIED	UNCLASSIFIED	UL

NANOCOMPOSITES SYNTHESIZED BY HIGH PRESSURE INJECTION OF POROUS DIELECTRICS AS OPTICAL MATERIALS

FINAL REPORT

TITO E. HUBER

JUNE 7, 1997

U.S. ARMY RESEARCH OFFICE

GRANT NO. DAAL03-91-G-0340

HOWARD UNIVERSITY

TABLE OF CONTENTS

A. INTRODUCTION

Recent advances in nanotechnology, such as novel synthesis and processing methods and scanning microscopies, have opened up research opportunities on materials with ultrafine microstructures. In particular, the design of composite materials consisting of a mixture of various phases in the nanometer range has flourished in the last few years.[1,2] Such heterogeneous forms of matter are especially interesting because one can tailor desired bulk properties by altering the constituents, their size distributions, or their relative concentrations. For example, the wavelength of visible light is a few thousand angstroms and generally exceeds such scales of inhomogeneity. Yet, as far as the optical properties of these systems are concerned, they behave as a continuum, and one may tune the dielectric properties in a way not possible with homogeneous systems.

Nanocomposites consisting of metals or semiconductors finely dispersed in a dielectric host represent a dramatic example of how the electronic properties of the conducting phase are modified by processing. For example, semiconductor and metal nanoparticle composites exhibit a modified optical response as a result of size and surface effects and have applications to selective optical filters, photothermal solar-energy converters, and nonlinear optical elements. Numerous practical applications require a high concentration of the active conducting phase. In this case, the electronic properties of the composite are strongly dependent upon the specifics of the microstructure. It is this interesting but relatively unexplored regime that we investigate.

The research described here focuses on the electrical and optical properties of dense conductor-insulator nanocomposites, i.e., those in which the conducting phase occupies a volume fraction of several tens percent. The composite preparation utilizes nanochannel dielectrics as host or template. The small channels in the host are filled with the conducting phase by high pressure injection of its melt. The template strategy has been successfully employed by others to chemically synthesize semiconductor and metal nanoparticles in microporous dielectrics[3-5] and in the cavities of zeolites.[6] More recently, experiments on capillary-induced filling of carbon nanotubes with lead have been reported.[7] In those cases the active conducting phase occupies a volume fraction typically less than one percent. The injection technique, on the other hand, can produce the dense

nanocomposites required for applications envisioned here which involve electrical transport.

This research ties in with recent developments in the fabrication of ultrasmall, uniform channel insulators which can be used as host for electronic and photonic materials.[8,9] Through this new approach to nanotechnology a new generation of quantum-related devices may be possible.

B. SUMMARY OF RESULTS

In the initial three-year period of this project we have prepared and characterized two distinct types of composites: nanocrystalline networks and nanowire arrays. We have performed structural, optical, and transport measurements which highlight the role of the microstructure on the electronic properties of the composite.

B.1 Microporous Template Injection

The template injection technique allows for the synthesis of conductor-insulator nanocomposites for both optical and electrical performance. Composites with highly reproducible properties are obtained in this way, since the impregnant "copies", to a large extent, the channel structure of the matrix. For the various metals and semiconductors we have investigated, we have found that an externally applied isostatic pressure is needed to overcome surface tension effects which prevent the melt from entering the narrow channels of insulating hosts. An estimate for the diameter d of the smallest channel filled at pressure P can be obtained from the Washburn equation:

$$d = - 4 \gamma \cos \alpha / P \qquad (1)$$

where γ is the surface tension of the liquid and α is the contact angle between the liquid and the insulator ($\alpha > 90^\circ$ for non-wetting liquids). Values for the surface tension of some

liquid metals and semiconductors of interest span the 100-600 dyne/cm range. Using a mid-range surface tension of 300 dyne/cm and assuming the least favorable case of complete non-wetting (α = 180°), the Washburn equation becomes d = 12 nm / P, where P is measured in kilobars. Then, for a modest pressure of , for example, 4 kbar all channels larger than 3 nm in diameter will be filled with the impregnant.

Most of the nanocomposites have been prepared with an injection apparatus we have designed and built ourselves. It is based on a high pressure pump using fluids as pressure transmission medium, and on an externally heated reactor with a maximum operating pressure of 4 kbar at 800 °C. The reactor and injection assembly are schematically illustrated in Figure 1.

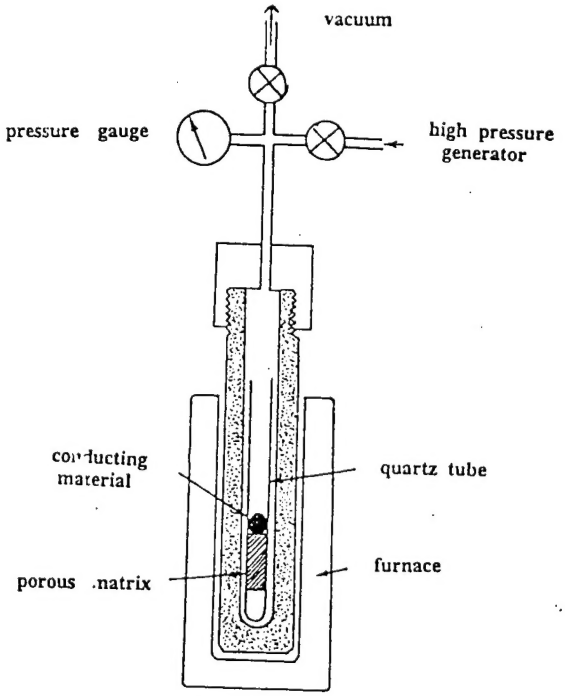

Figure 1: Injection reactor

Details about the apparatus construction and operation have been reported previously.[10] Briefly, the reactor is heated in vacuum to a temperature above the metal (or semiconductor) melting point. The metal melts and surrounds the porous matrix making a tight seal. A pressure-transmitting fluid is then introduced and its pressure gradually raised, the molten metal is then pushed into the matrix channels by the isostatic pressure. When the injection is complete the reactor is cooled and the metal solidifies

inside the channels, the high pressure is then removed. Using water or oil as pressure-transmitting fluid may cause oxidation or contamination. In such case, the porous matrix and metal are initially packed in an evacuated, thin-wall, sealed metal capsule which collapses under the high pressure. We have prepared composite samples of typical dimensions of 1 cm. From gravimetric measurements performed on numerous samples we have determined that the impregnant fills 92-97% of the pore volume for the smallest, nanometer-size channels.

A fundamental limit of the high temperature injection process is established by the sintering of the template which takes place at these temperatures. Figure 2 shows how the porosity decreases with temperature for two templates we have used: porous silica (6 nm average pore size, interconnected pores)[11] and nanochannel alumina (parallel channels, 200 nm in diameter)[12]. For these templates, the choice of impregnants is limited to materials with a melting point below 1,400 °C.

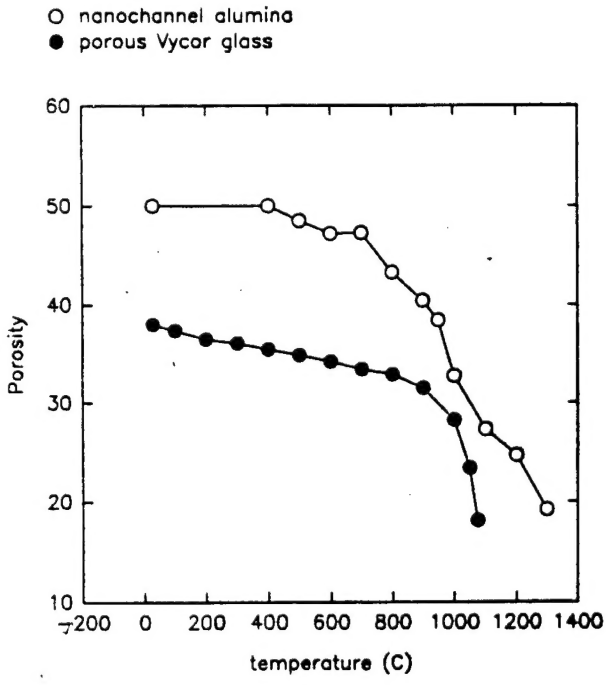

Figure 2: Template sintering.

B.2 Network Nanocomposites

We have prepared and studied nanocomposites where the conducting phase is in the form of a network of strands as small as 6 nm in diameter. Commercial silica glasses which support an interconnected array of channels of average pore diameter ranging from 5.6 nm to 300 nm and 30% to 70% porosity were used as template. The porous silicae were characterized by nitrogen adsorption porosimetry, to determine their pore size distribution, and scanning electron microscopy (SEM). Figure 3 shows a SEM micrograph of a porous silica glass monolith commercially available under the trade name Vycor (Corning Inc.). The sample shown in Figure 3 has a 5.6 nm average pore diameter, too small to be resolved by the SEM, and 33% porosity.[13]

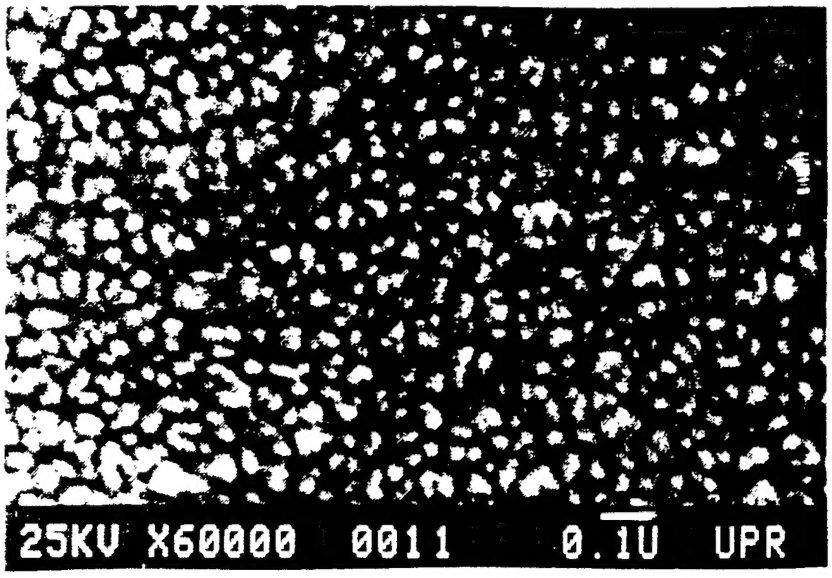

Figure 3: Porous Vycor glass. The silica appears as light clusters, the channels in dark.

The structure of the network composites was characterized by small angle X-ray scattering (SAXS), X-ray diffraction (XRD), and Raman spectroscopy. SAXS

measurements were made at the National Center for Small Angle Scattering in Oak Ridge, TN. SAXS is an excellent technique for investigating porous media on a scale of lengths between about 1 and 200 nm. Figure 4 shows the SAXS spectra of the porous silica of Figure 3 and of a selenium-silica composite prepared from it. Selenium has a relatively low atomic number and a Se-SiO_2 composite sample a few tenths of a millimeter thick transmits a significant fraction of the incident X-rays.

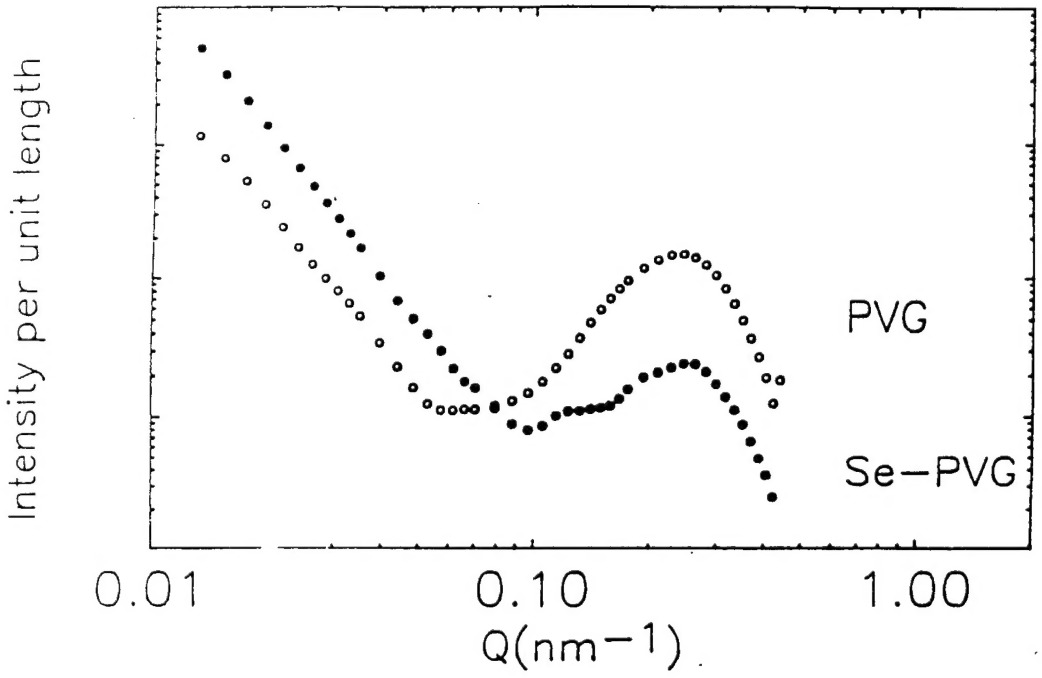

Figure 4: SAXS from porous Vycor Glass (PVG) and from a Se-PVG composite.

The scattering wavevector is:

$$q = 2\pi \cos\eta / \lambda \qquad (2)$$

where η is the scattering angle and λ = 0.1542 nm is the X-ray wavelength. The intermediate spectral region $0.1 < q < 0.5$ nm^{-1} is related to the average size of the grains that make the Vycor.[14] The spectra show a peak in this region in both the bare Vycor and

the composite. From the rough criterion that the scattering shows a maximum at $q_m = 2\pi / L$, where L is the characteristic size of the particles that form the material, we obtain L = 30 nm for both the bare Vycor and the composite. This agrees fairly well with the silica particle size seen in the micrograph of Figure 3. The observation that the silica particle size is the same in the bare Vycor and in the composite indicates that the microstructure of the template is essentially preserved after the injection process.

The XRD spectrum from a Te-SiO_2 composite prepared from a 5.6 nm channel diameter silica is shown in Figure 5. The spectrum is typical for the various network composites investigated. In all cases the impregnant is found to retain the crystal structure of the bulk.

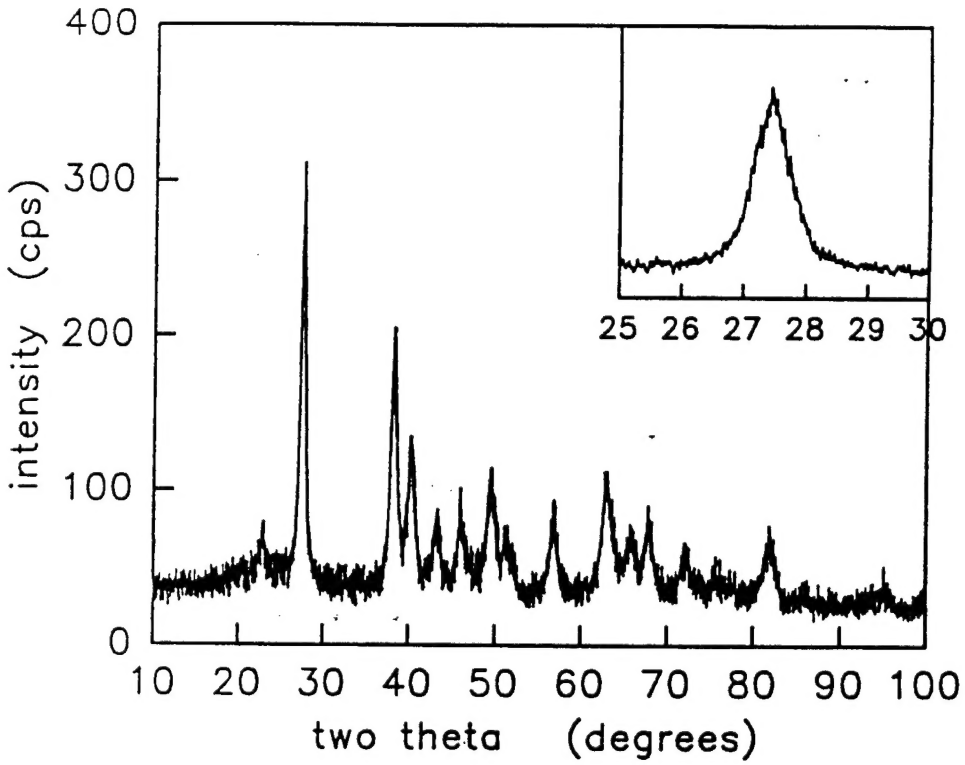

Figure 5: Theta-two theta X-ray scan from a Te/SiO_2 network.

An estimate for the average semiconductor crystallite size D is obtained from the

widths of the XRD peaks through Scherrer's equation:

$$D = K \lambda / \beta \cos\theta \qquad (3)$$

where $\lambda = 0.1542$ nm is the X-ray wavelength, β is the contribution to the linewidth due to the finite crystallite size, 2θ is the diffraction angle, and K is a factor related to the crystallite shape which could assume values between 0.7 and 1.7 and is taken here to be one. After correcting the measured linewidths for the finite instrumental resolution and for the X-ray doublet broadening, crystallite sizes obtained from peaks corresponding to different sets of crystal planes were found to be about the same, indicating that there is no preferential orientation of the crystallites along the network strands. Values for D obtained from Equation (3) along with values for the lattice constants relative to the bulk, $\delta a/a$, obtained from the angular position of the XRD peaks are listed in Table I.

Table 1: Crystal parameters of the conducting phase in the 5.6 nm network composites

	$\delta a/a$	D (nm)
Se		amorphous
Te	$\leq 1 \times 10^{-3}$	14
GaSb	-1.5×10^{-3}	19
In	2×10^{-3}	25

The rather small widths of the XRD peaks suggest that there is a significant degree of long range crystalline order, and that the average network crystallite size is not necessarily limited by the 5.6 nm channel size.

Raman spectroscopy is a non-destructive technique which has proved to be most useful for the study of the vibrational and structural properties of microcrystalline

materials. We have performed Raman measurements on the network composites which, when correlated to the results form XRD experiments, provide further insight into the complex microstructure. The first order Raman spectra of the 5.6 nm silica composites are shown in Figure 6.

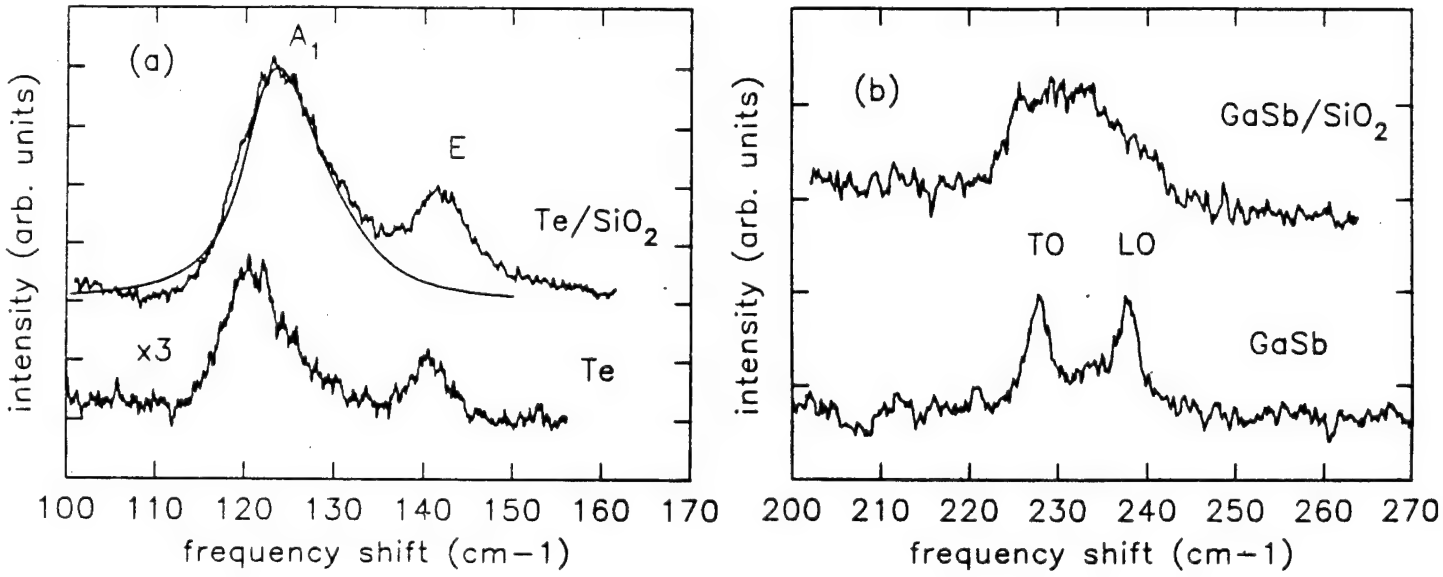

Figure 6: Raman spectra of (a): Te/SiO_2, and (b): $GaSb/SiO_2$ network composites. The spectra of the bulk semiconductors are also shown. The smooth line fit to the A_1 mode of Te in the composite corresponds to a phonon-confinement calculation as described in the text.

The Raman peaks of the composites show broadenings and, for the strong A_1 mode of Te, a high energy shift and tail. This shift and asymmetry are interpreted as resulting from phonon confinement in the nanocrystals. For a finite size crystal,

localization of the phonon wave function causes the relaxation of the k=0 Raman selection rule, i.e., the phonon wavevector k is not a good quantum number in a finite lattice. This results in contributions to the Raman signal from phonons away from the center of the Brillouin zone. The shift and width of the Raman peaks are then related to the phonon dispersion relation of the material and the crystallite size and shape. Shown in Figure 6.a is the result from a standard model calculation of the Raman lineshape for a spherical crystallite.[15] The best fit is obtained for a Te crystallite of 10 nm diameter, which corresponds quite closely with the 14 nm crystallite size obtained from the XRD measurements (Table 1). However, if cylindrical crystallites are assumed, an equally good fit is obtained for a 5.6 nm diameter, the channel size of the silica matrix. It does not seem possible to unambiguously determine the crystallite shape from a fit to the Raman line shape in this circumstance.

We have also studied the melting/freezing phase transition of the network composites. The calorimetry experiments were done in collaboration with Prof. K. Unruh of the University of Delaware. The thermodynamics of the confined metal (or semiconductor) is found to be quite different from that of the macroscopic bulk. For instance, an indium network of strands 2 nm in diameter will melt at room temperature (versus 156 °C for bulk In) and its latent heat of melting can be less than a third of its bulk value.[16] While calorimetric studies of the solid-liquid transition of complex organic fluids in porous matrices have been previously done by other authors, this is the first time a metal element has been investigated. The results are relevant to the potential use of nanocomposites in nonlinear optics applications involving high intensity radiation where the thermal stability of the material can be an issue.

The intricate microstructure of the network composites often results in ambiguities when trying to interpret experimental data on the size-dependent properties according to theoretically tractable, yet simplified, geometrical models. This is evidenced, for example, when probing for carrier confinement effects on the optical properties of small-effective-mass semiconductor networks. Figure 7 shows the room temperature absorption edge of a GaSb/SiO_2 network of strands 5.6 nm in diameter and of bulk GaSb.

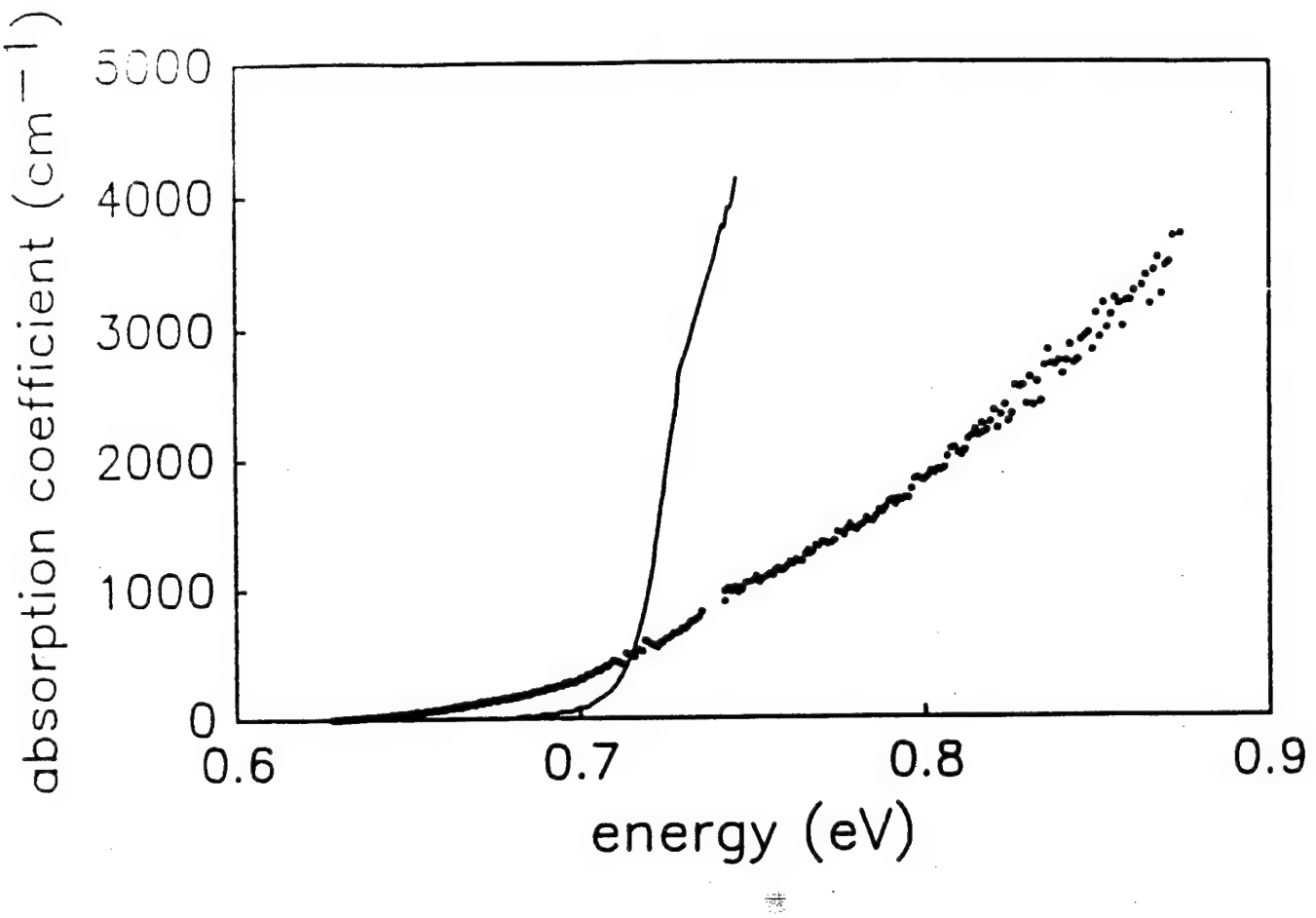

Figure 7: Absorption of a 5.6 nm GaSb network (dots) and of bulk GaSb (solid line).

Bulk GaSb shows a sharp absorption edge at photon energies corresponding to the direct energy gap at 0.71 eV. The absorption spectrum of the nanocomposite is blue-shifted from that of the bulk and shows a long absorption tail. An estimate for the magnitude of carrier confinement energies in this case can be obtained by considering that the strand radius R = 2.8 nm is smaller than or comparable to the effective Bohr radii of electrons (15 nm), holes (2 nm and 12 nm for heavy and light holes,respectively) and of excitons (17 nm and 27 nm for the heavy-hole- and light-hole-exciton) in GaSb. In this limit, the lowest energy of an electron-hole pair is larger than that in the bulk due to

independent size-quantization of the electron and of the hole motion.[17] If a simplified model of cylindrical strands is assumed and possible polarization effects arising from the dielectric discontinuity are disregarded, the absorption threshold can be calculated from the energy levels of a particle in an infinite cylindrical potential well. It is blue-shifted from the bulk value by an amount $E = 5.78\ \hbar^2 / 2\ \mu\ R^2 = 0.78$ eV, with μ the reduced electron-heavy hole effective mass.

Clearly, the measured shift of the optical absorption of the composite is significantly smaller than the calculated value. This likely results from a crystallite-size distribution and from the network microstructure, which is more complex than the simple model of cylinders.

B.3 Nanowire Array Composites

We have prepared a class of composites consisting of a high density array of parallel, nanometer-size, metallic wires embedded in a dielectric matrix. The composite preparation uses a porous dielectric with a regular nanochannel structure as matrix for injection. In contrast to the porous silicae which support a random network of pores, the regular nanochannel matrices allow for the preparation of composites where physical properties are easier to interpret and more amenable to theoretical treatments.

The template used for the synthesis of the nanowire composite is a porous Al_2O_3 in the form of a plate several centimeters in diameter and about 55 μm thick, which supports an array of parallel, mostly non-interconnected channels running perpendicular to the plate surface. Figure 8 shows a SEM photograph of a commercially available plate of 200 nm nominal channel diameter and about 50% porosity. The photograph illustrates the tubular channels. From analysis of micrographs of the plate top surface we determine a channel diameter of 258 ± 46 nm and a channel density of 5-7 x 10^8 cm^{-2}. The sintering of the nanochannel alumina with temperature is illustrated in Figure 2.

Figure 8: Cross-section view of a 200 nm nominal channel diameter alumina obtained by cleaving the plate.

Figure 9 shows micrographs of a Te nanowire composite prepared by injection of the Al_2O_3 template, the semiconducting phase appears as light areas. For the cross-section view the 50 μm-thick plate was cleaved and the surface thus exposed was mechanically polished.

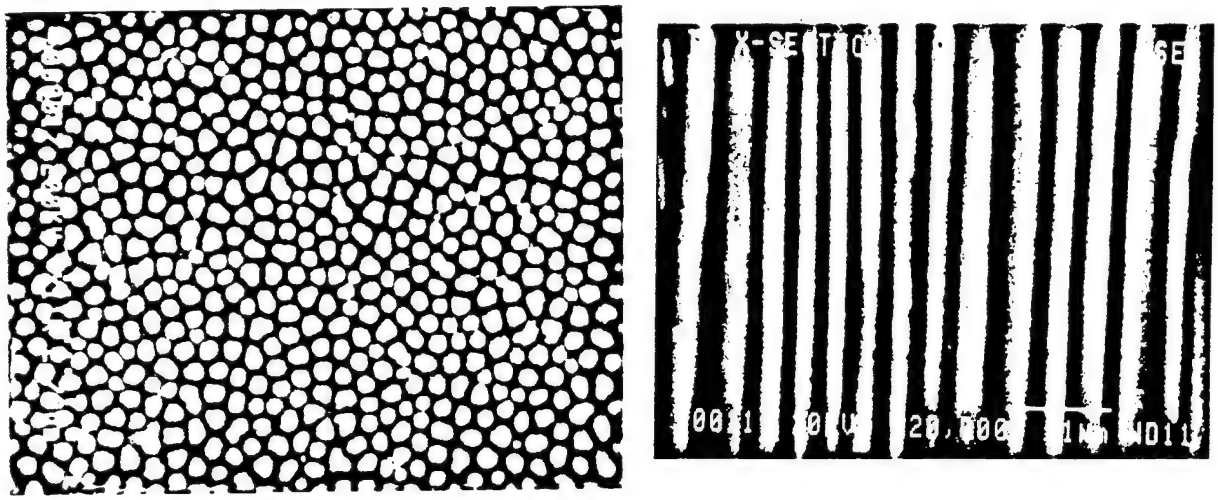

(a) (b)

Figure 9: Te nanowire composite prepared from a 200 nm channel alumina plate. (a) top view. (b) cross-section.

XRD measurements on the nanowire composites show that for certain materials and under certain preparation conditions the nanowires are highly crystalline and have a strong preferential crystal orientation relative to their length. This is illustrated in Figure 10 for a Te/Al_2O_3 nanowire composite where the diffraction spectrum is dominated by the (1010) set of crystal planes, indicating that the 200 nm diameter Te wires are oriented with the trigonal c-axis perpendicular to the wire length. The broad background features are from the nanocrystalline, almost glassy, alumina template.

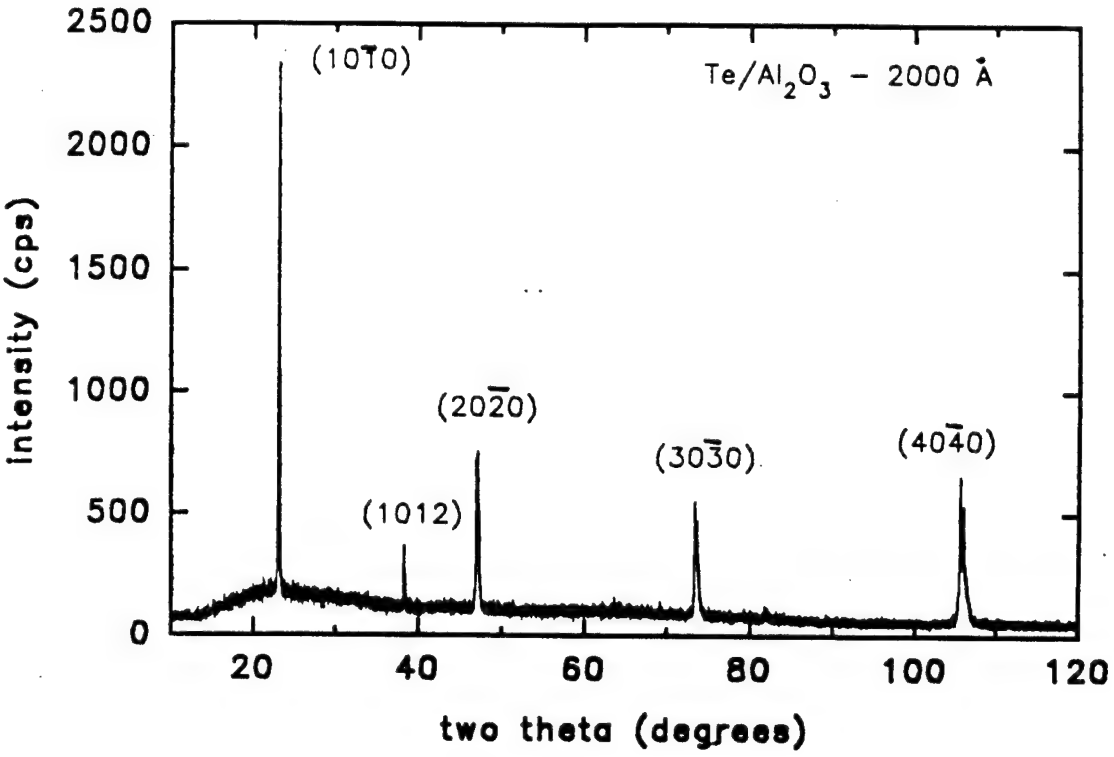

Figure 10: XRD spectrum of 200 nm Te nanowires

These preliminary results suggest the possibility of fabricating arrays of oriented crystal nanowires, the experimental conditions for crystal orientation will be established as part of the proposed research.

Some applications of the nanowire composites, such as nanochannel charge transfer plates for microelectronic and photonic devices (spatial light modulators),[18] will tap their potential to create substantial electric field patterns over the sample surface. We have teamed up with researchers at Digital Instruments, Santa Barbara, CA, a company

at the leading edge of scanning force microscopy instrumentation, to develop a scanning force microscope that allows for the mapping of the electric fields at the surface of a composite with nanometer resolution. In this way, we have obtained high spatial resolution images of the strong, short range electric fields generated by the nanowires when charged. The results of this work are described in an article in Science magazine and are also featured in the Research News section of Science.[19]

For the electric field measurements, a small voltage is applied between the nanowires and the cantilever tip of a scanning force microscope. The tip is set to oscillate at a frequency near its resonance frequency. When the cantilever encounters a vertical electric field gradient, the effective spring constant is modified, shifting its resonance frequency. By recording the amplitude of the cantilever oscillations while scanning the sample surface, an image revealing the strength of the electric force gradient is obtained. This image, however, may also contain topographical information, making it difficult to separate the two effects. This is circumvented by taking two passes over each scan line. On the first pass, a topographical image is taken with the cantilever tapping the surface and the information is stored in memory. On the second pass, the tip is lifted to a selected separation between the tip and local surface topography, such that the tip does not touch the surface. By using the stored topographical data as feedback, the separation remains constant. In this second pass, cantilever oscillation amplitudes are sensitive to electric force gradients without being influenced by topographic features. This two-pass measurement process is recorded for every scan line, producing separate topographic and electric force images.

Shown in Figure 11.a is the topographic image of a nanowire composite where the Al_2O_3 has been etched so that the wires protrude slightly. Higher topography features appear as lighter areas. Dark lines in this image are from the mechanical polishing. The corresponding image of the electric force gradient taken with a lift height of 30 nm is shown in Figure 11.b. Contours of constant electric force gradient taken from this image are shown in Figure 11.c. Note that some of the nanowires that appear in the topographic image are missing from the electric field image. This is because either electrical contact to these nanowires has failed or electrical conduction along the wire length has been interrupted.

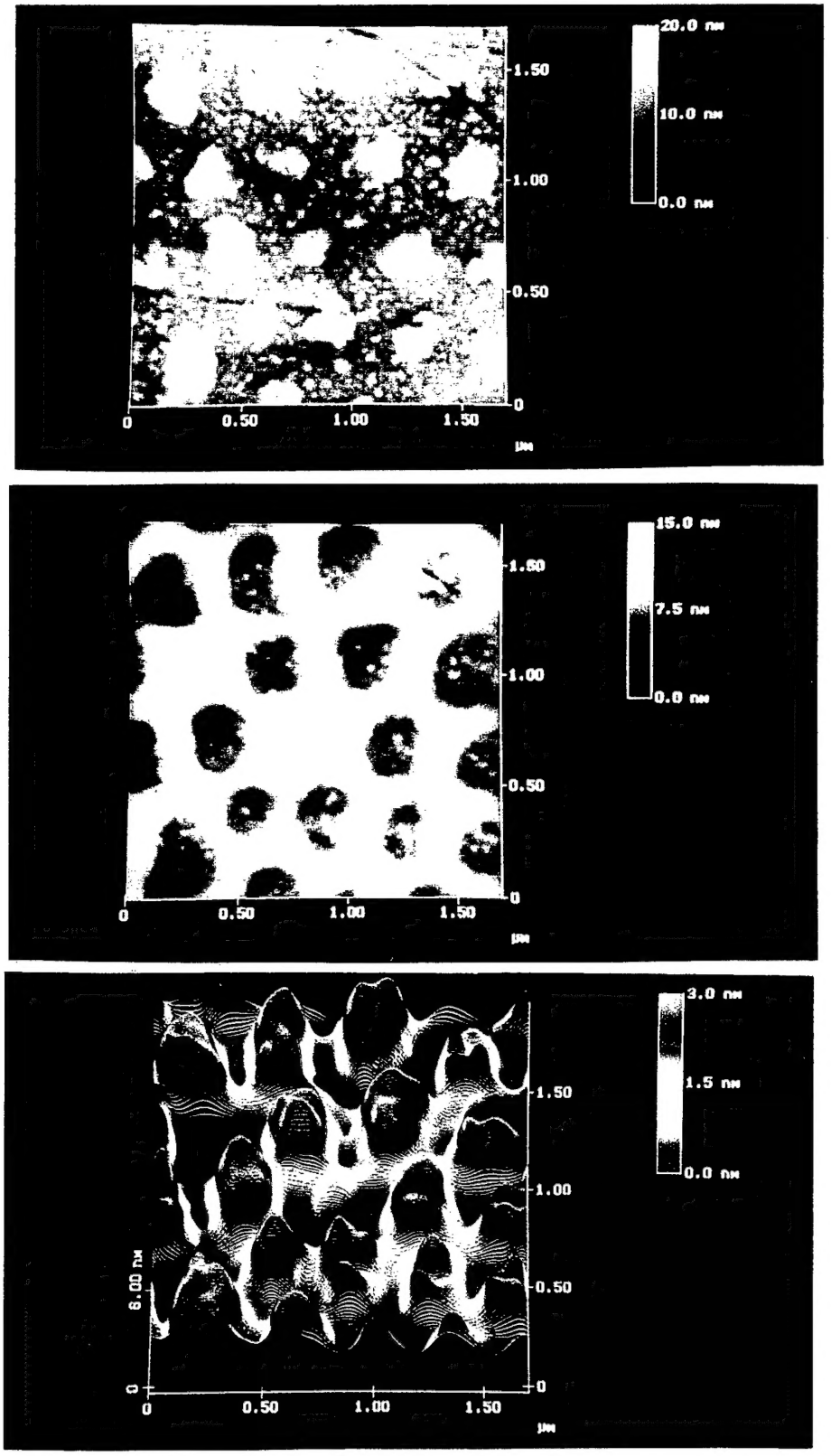

Figure 11: (a) AFM topographic image of the nanowire composite. (b) Electric force gradient image. (c) Contours of constant electric force gradient.

In the electric field images the amplitude of the cantilever oscillations is found to be very large for small lift heights, and the images fade at separations larger than 80 nm. This is consistent with previous reports of a strong dependence of the tip-surface force on the vertical separation. More work needs to be done to understand this quantitatively.

The nanowire composites can be utilized as building blocks for high density electrical multifeedthroughs and photosensing arrays. Also, the electrically conductive composites can be microengineered to become optically transmissive. The research described in the following sections will focus on this novel class of composites.

C. PUBLICATIONS

1. "Superconducting Properties of Indium in the Restricted Geometry of Porous Vycor Glass", M.J. Graf, T.E. Huber, and C.A. Huber, *Physical Review* **B45**, 3133 (1992).
2. "Size-Dependent Melting and Freezing Behavior of Indium Metal Confined in Porous Glasses", K.M. Unruh, J.F. Sheehan, T.E. Huber, and C.A. Huber, *Nanostructured Materials* **3**, 425 (1993).
3. "Synthesis and Optical Properties of Dense Semiconductor-Dielectric Nanocomposites", C.A. Huber, J.A. Lubin, W.H. Yang, and T.E. Huber, *Journal of Physics: Condensed Matter* **5**, A337 (1993).
4. "Melting and Freezing Behavior of Indium Metal in Porous Glasses", K.M. Unruh, T.E. Huber, and C.A. Huber, *Physical Review* **B48**, 9021 (1993).
5. "Raman and X-Ray Scattering from Dense Semiconductor-Dielectric Nanocomposites", W.H. Yang, T.E. Huber, J.A. Lubin, G.E. Walrafen, and C.A. Huber, *Nanophase and Nanocomposite Materials*, S. Komarneni, J.C. Parker, and G.J. Thomas, eds., *Materials Research Society Symposia Proceedings* **286**, 419 (1993).
6. "Nanowire Array Composites", C.A. Huber, T.E. Huber, M. Sadoqi, J.A. Lubin, S. Manalis, and C.B. Prater, *Science* **263**, 800 (1994).
7. "Microengineered Conducting Composites from Nanochannel Templates", C.A.

Huber, M. Sadoqi, T. Huber, and D. Chacko, invited contribution to *Advanced Materials*, submitted (1994).

D. PARTICIPATING PERSONNEL

Senior personnel: Prof. Tito Huber, Howard University and Polytechnic University
Dr. Carmen Huber, Naval Surface Warfare Center - White Oak

Graduate Students: Mr. Jean Lubin, M.S. student, Howard University
Ms. Debra Chacko, M.S. student, Howard University
Mr. Mostafa Sadoqi, Ph.D. degree, Polytechnic U., Dec. 1994

Undergraduate Students: Mr. Mpoyo George, Howard University

E. INVENTIONS

1. "Method of Making a Photodetector Array Having High Pixel Density", C.A. Huber, T.E. Huber, T-K. Chu, and N. Caviris, U.S. Patent No. 5;328,853, July 12, 1994.
2. "Method of Making Ultrahigh Density Charge Transfer Device", C.A. Huber, T.E. Huber, and N. Caviris, Appl. No. 59,766, filed May 11, 1993.
3. "Photodetector Array Having High Pixel Density", C.A. Huber, T.E. Huber, T-K. Chu, and N. Caviris, Appl. No. 230,461, Filed April 20, 1994.

The above inventions have been highlighted in the Inventors Hall of Fame in Akron, OH.

F. BIBLIOGRAPHY

1. An overview can be found in the *Proceedings of the First International Conference on Nanostructured Materials*, Cancun, 1992, M.J. Yacaman, T. Tsakalakos, and B.H. Kear, eds., *Nanostructured Materials* **3** (1993).

2. Rustum Roy, *Nanophase and Nanocomposite Materials*, S. Komarneni, J.C. Parker, and G.J. Thomas, eds, *Mat. Res. Soc. Symp. Proc.* **286**, 241 (Materials Research Society, Pittsburgh, 1993), and references therein.
3. N.F. Borrelli and J.C. Luong, *Materials and Technologies for Optical Communications*, Cannes, 1987, *Proc. SPIE-Int. Soc. Opt. Eng.* **866**, 104 (1988).
4. B.L. Justus, R.J. Tonucci, and A.D. Berry, *Appl. Phys. Lett.* **61**, 3151 (1992).
5. M.J. Tierney and C.R. Martin, *J. Phys. Chem.* **93**, 2878 (1989).
6. G.D. Stucky and J.E. Mac Dougall, *Science* **247**, 669 (1990) and references therein.
7. P.M. Ajayan and S. Iijima, *Nature* **361**, 333 (1993).
8. R.J. Tonucci, B.L. Justus, A.J. Campillo, and C.E. Ford, *Science* **258**, 783 (1992).
9. C.T. Kresge, M.E. Leonowicz, W.J. Roth, J.C. Vartuli, and J.S. Beck, *Nature* **359**, 710 (1992).
10. C.A. Huber and T.E. Huber, *J. Appl. Phys.* **64**, 6588 (1988).
11. T.H. Elmer, I.D. Chapman, and M.E. Nordberg, *J. Phys. Chem.* **66**, 1517 (1962).
12. D. Chacko and C.A. Huber, to be published.
13. T.E. Huber and C.A. Huber, *Fractal Aspects of Materials*, J.H. Kaufman, J.E. Martin, and P.W. Schmidt, eds., *Mat. Res. Soc. Symp. Proc.* **EA-20**, 97 (1989).
14. T.E. Huber, P.W. Schmidt, J.S. Lin, and C.A. Huber, *Scaling in Disordered Materials: Fractal Structure and Dynamics*, J.P. Stokes, M.O. Robbins, and T.A. Witten, eds., *Mat. Res. Soc. Symp. Proc.* **EA-25**, 207 (1990) and to be published.
15. W.H. Yang, T.E. Huber, J.A. Lubin, G.E. Walrafen, and C.A. Huber, Nanophase and Nanocomposite Materials, S. Komarneni, J.C. Parker, and G.J. Thomas, eds., *Mat. Res. Soc. Symp. Proc.* **286**, 419 (Materials Research Society, Pittsburgh, 1993).
16. K.M. Unruh, T.E. Huber, and C.A. Huber, *Phys. Rev.* **B48**, 9021 (1993).
17. Al.L. Efros and A.L. Efros, *Sov. Phys. Semicond.* **16**, 772 (1982).
18. C.A. Huber, T.E. Huber, and N. Caviris, *Ultrahigh Density Charge Transfer Plate Device*, patent pending.
19. C.A. Huber, T.E. Huber, M. Sadoqi, J.A. Lubin, S. Manalis, and C.B. Prater, *Science* **263**, 800 (1994).